Chaos, Solitons and Fractals 169 (2023) 113249

Contents lists available at ScienceDirect

Chaos, Solitons and Fractals

journal homepage: www.elsevier.com/locate/chaos

Computer simulation of the nonhomogeneous zebra pattern formation using a mathematical model with space-dependent parameters

Junxiang Yang, Junseok Kim *

Department of Mathematics, Korea University, Seoul 02841, Republic of Korea

ARTICLE INFO

Keywords:
Turing pattern
Lengyel–Epstein model
Nonhomogeneous zebra pattern formation

ABSTRACT

In this study, we present a mathematical model with space-dependent parameters and appropriate boundary conditions which can simulate the realistic nonhomogeneous zebra pattern formation. The proposed model is based on the Lengyel–Epstein (LE) model and the finite difference method is used to solve the governing equation with appropriate boundary and initial conditions on a complex zebra domain. We focus on generating nonhomogeneous pattern of the common plains zebra (E. burchelli), which is geographically widespread species of zebra. Using the space-dependent parameters in the model, we can simulate the zebra pattern formation with various width stripes.

1. Introduction

It is still an unresolved problem how spatial pattern formation emerges in real biological systems. In 1952, a mathematician Alan Turing proposed a partial differential equation for pattern formation in the natural world and hypothesized that spatially heterogeneous patterns could arise with diffusion driven instability [1–6]. The Turing instability has been applied to many fields such as zebrafish figment pattern formation [7], multi-scale regular vegetation patterns [8], Turing patterns on radially growing domains [9], Turing patterns in a dye-doped twisted nematic layer [10], and self-organization in cell biology [11]. In [12], the author developed a novel numerical method for solving the Caputo and Fabrizio fractional equations.

In this study, we focus on a mathematical model for simulating zebra pattern formation. There are three main species of zebra: E. burchelli, E. zebra, and E. grevyi [13]. Graván and Lahoz-Beltra [14] computed the evolution of two hypothetical morphogens that diffuse across a grid representing the zebra skin pattern in an embryonic state. Jeong et al. [15] computationally studied the zebra skin pattern formation on the surface of a zebra model in 3D space using a narrow band domain with the closet point method. Rasheed [16] presented a novel mathematical equation of the reaction–diffusion (RD) system which satisfies Turing conditions and simulates real pattern formation in nature. In [17], the authors simulated the evolution of two morphogens for modeling the zebra skin pattern formation. Kim et al. [18] presented an explicit Euler method for the pattern formation on evolving surfaces using the Laplace–Beltrami operator over triangulated surface in the three-dimensional space.

Although there have been many research works about the zebra pattern formation until now, most of patterns have a single width between patterns. However, in real zebra skin, there are multiple widths between patterns as we can observe in Fig. 1.

The main purpose of this study is to present a mathematical model with space-dependent parameters and appropriate boundary conditions which can simulate the realistic nonhomogeneous zebra pattern formation. The paper is organized in the following manner. In Section 2, the proposed mathematical model is presented. In Section 3, we describe the numerical solution algorithm.

2. Proposed mathematical model

In this study, we propose a novel reaction–diffusion (RD) equation with space-dependent parameters and appropriate boundary conditions:

$$\frac{\partial u}{\partial t} = D_u \Delta u + f(u,v) = D_u \Delta u + k_1 \left(v - \frac{uv}{1+v^2} \right), \tag{1}$$

$$\frac{\partial v}{\partial t} = D_v \Delta v + g(u,v) = D_v \Delta v + k_2 - v - \frac{4uv}{1+v^2}, \tag{2}$$

where $u(x,y,t)$ and $v(x,y,t)$ are two concentrations (morphogens) of an inhibitor and an activator at two-dimensional position $(x,y) \in \Omega$ and time t, respectively. Here, $f(u(x,y,t),v(x,y,t))$ and $g(u(x,y,t),v(x,y,t))$ describe the reaction kinetics of the morphogens represented by $u(x,y,t)$ and $v(x,y,t)$ [1]. Here, D_u and $D_v(x,y)$ are the diffusion coefficients of u and v, respectively; and $k_1(x,y)$ and k_2 are positive values related to the

* Corresponding author.
E-mail address: cfdkim@korea.ac.kr (J. Kim).
URL: https://mathematicians.korea.ac.kr/cfdkim (J. Kim).

https://doi.org/10.1016/j.chaos.2023.113249
Received 27 November 2022; Received in revised form 21 January 2023; Accepted 8 February 2023
Available online 15 February 2023

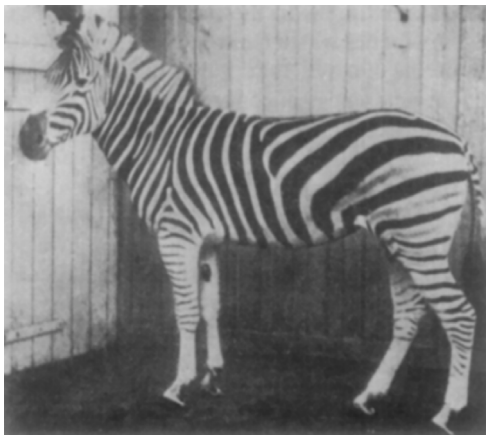

Fig. 1. Plains (Equus burchelli) zebra.
Source: Reprinted from Bard [21] with permission from Academic Press Inc.

feed concentrations. We should note that both $D_v(x, y)$ and $k_1(x, y)$ are space-dependent parameters. If we use all constant parameters [19], then we can only model regular pattern formations. However, most mammals show a regional variation of stripe spacing [20]. By choosing different values of $D_v(x, y)$ and $k_1(x, y)$ on different positions, we can model varying stripe pattern widths of a zebra. Let u^* and v^* be the homogeneous steady state solutions of Eqs. (1) and (2), i.e.,

$$f(u^*, v^*) = 0 \text{ and } g(u^*, v^*) = 0. \tag{3}$$

Then, the solutions of Eq. (3) are given as

$$u^* = 1 + 0.04k_2^2 \text{ and } v^* = 0.2k_2. \tag{4}$$

We note that Eqs. (1) and (2) are not general and there are many other reaction–diffusion equations which can generate patterns through the Turing instability. For simplicity of exposition, we chose one of them for illustrating the possibility of nonhomogeneous patterns observed in the real world.

3. Numerical solution algorithm

We present a numerical algorithm for the Lengyel–Epstein model on the two-dimensional domain, $\Omega = (L_x, R_x)\times(L_y, R_y)$. Let N_x and N_y be positive integers, $h = (R_x - L_x)/N_x = (R_y - L_y)/N_y$ be the uniform mesh size, and $\Omega^h = \{(x_i, y_j) | x_i = L_x + (i - 0.5)h,\ y_j = L_y + (j - 0.5)h,\ 1 \le i \le N_x,\ 1 \le j \le N_y\}$ be the discrete domain. Let $u_{ij}^n = u(x_i, y_j, n\Delta t)$, $v_{ij}^n = v(x_i, y_j, n\Delta t)$, $k_{1,ij} = k_1(x_i, y_j)$, and $D_{v,ij} = D_v(x_i, y_j)$, where $\Delta t = T/N_t$ is the time step, T is the final time, and N_t is the total number of time steps. We consider the discretization of the reaction–diffusion system (1) and (2) using an explicit scheme for simplicity of exposition,

$$\frac{u_{ij}^{n+1} - u_{ij}^n}{\Delta t} = D_u \Delta_h u_{ij}^n + k_{1,ij}\left(v_{ij}^n - \frac{u_{ij}^n v_{ij}^n}{1 + (v_{ij}^n)^2}\right), \tag{5}$$

$$\frac{v_{ij}^{n+1} - v_{ij}^n}{\Delta t} = D_{v,ij} \Delta_h v_{ij}^n + k_2 - v_{ij}^n - \frac{4u_{ij}^n v_{ij}^n}{1 + (v_{ij}^n)^2}, \tag{6}$$

where $\Delta_h u_{ij} = (u_{i+1,j} + u_{i-1,j} + u_{i,j+1} + u_{i,j-1} - 4u_{ij})/h^2$. We note that there are many efficient implementations with some complexity such as the graphics process unit (GPU) computing using compute unified device architecture (CUDA) [22].

4. Numerical experiments

4.1. Pattern formation on a rectangular domain

We first numerically solve Eqs. (1) and (2) on a two-dimensional rectangular domain $\Omega = [0, 10] \times [0, 10]$ using $D_u = 1$, $k_2 = 11$, a mesh grid 101×101, $h = 0.1$, and $\Delta t = 0.1h^2$. Here, periodic boundary conditions in each direction are used. Initial conditions for u and v are $u(x, y, 0) = u^* + 0.1\text{rand}(x, y)$, $v(x, y, 0) = v^* + 0.1\text{rand}(x, y)$, where $u^* = 1 + 0.04k_2^2$, $v^* = 0.2k_2$, and $\text{rand}(x, y)$ is a random number between -1 and 1. Fig. 2 shows different pattern formations with different k_1 and D_v values in the discrete governing equations at time $t = 100000\Delta t$. We can observe spots and stripes depending on the parameters as shown in [23]. The parameter sets leading to pattern formation are usually determined by a linear stability analysis [24].

4.2. Pattern formation on a zebra shaped domain

Fig. 3(a) shows the schematic illustration of subdomains Ω_1, Ω_2, and Ω_3, where different parameter values are defined. Let $\Omega = (0, 29)\times(0, 22)$ be the domain which embeds all subdomains, i.e., $\Omega_i \subset \Omega$ for $i = 1, 2, 3$. Let us define the space-dependent parameters as follows:

$$D_v(x, y) = 0.012, \quad k_1(x, y) = 12 \quad \text{in } \Omega_1, \tag{7}$$

$$D_v(x, y) = 0.05, \quad k_1(x, y) = 4 \quad \text{in } \Omega_2, \tag{8}$$

$$D_v(x, y) = 0.007, \quad k_1(x, y) = 30 \quad \text{in } \Omega_3. \tag{9}$$

Fig. 3(b) shows domain boundaries Γ_1 and Γ_2, where Dirichlet boundary conditions are applied.

$$u(x, y, t) = u^*, \quad v(x, y, t) = v^* \quad \text{on } \Gamma_1, \tag{10}$$

$$u(x, y, t) = 1.01u^*, \quad v(x, y, t) = 1.01v^* \quad \text{on } \Gamma_2, \tag{11}$$

It is well known that the pattern formations are dependent on both the initial condition and biochemical details [21]. In this study, as the initial condition, we set the equilibrium state $u(x, y, 0) = u^*$ and $v(x, y, 0) = v^*$ on the zebra domain expect two lines. Fig. 3(c) shows two line segments where initial trigger values are defined: $u(x, y, 0) = 1.2u^*$ and $v(x, y, 0) = 1.2v^*$. We take the minimum number of intervention for the initial configuration to demonstrate the ability of the governing equation to generate the zebra pattern formation. Fig. 4(a)–(d) show the snapshots of the temporal evolution of the realistic zebra pattern formation at times $t = 10000\Delta t$, $15000\Delta t$, $25000\Delta t$, and $70000\Delta t$, respectively. Here, $h = 0.1$ and $\Delta t = 0.1h^2$ are used.

4.3. Effect of parameter profiles

Now, we consider the effect of parameter profiles on the pattern formation. Fig. 5(a) and (b) show the two methods of the space-dependent parameters of the sharp jump and smooth profiles, respectively. In Fig. 5, the top and bottom rows are $D_v(x, y)$ and $k_1(x, y)$, respectively.

Fig. 6(a)–(d) show snapshots of the temporal evolution of the zebra pattern formation using the smooth space-dependent parameters $D_v(x, y)$ and $k_1(x, y)$ as shown in Fig. 5(b) at times $t = 10000\Delta t$, $15000\Delta t$, $25000\Delta t$, and $70000\Delta t$, respectively. The parameter values are the same as in the previous subsection except $D_v(x, y)$ and $k_1(x, y)$. We can observe much smoother transition patterns across different subdomains.

5. Conclusions

In this study, it was shown that we can simulate the zebra pattern formation with various width stripes using the space-dependent parameters in the model and appropriate boundary conditions. From this result, we can make a hypothesis about different patterns among zebras. We postulate different pattern formations can arise under different local conditions. The proposed method can be used in systematically

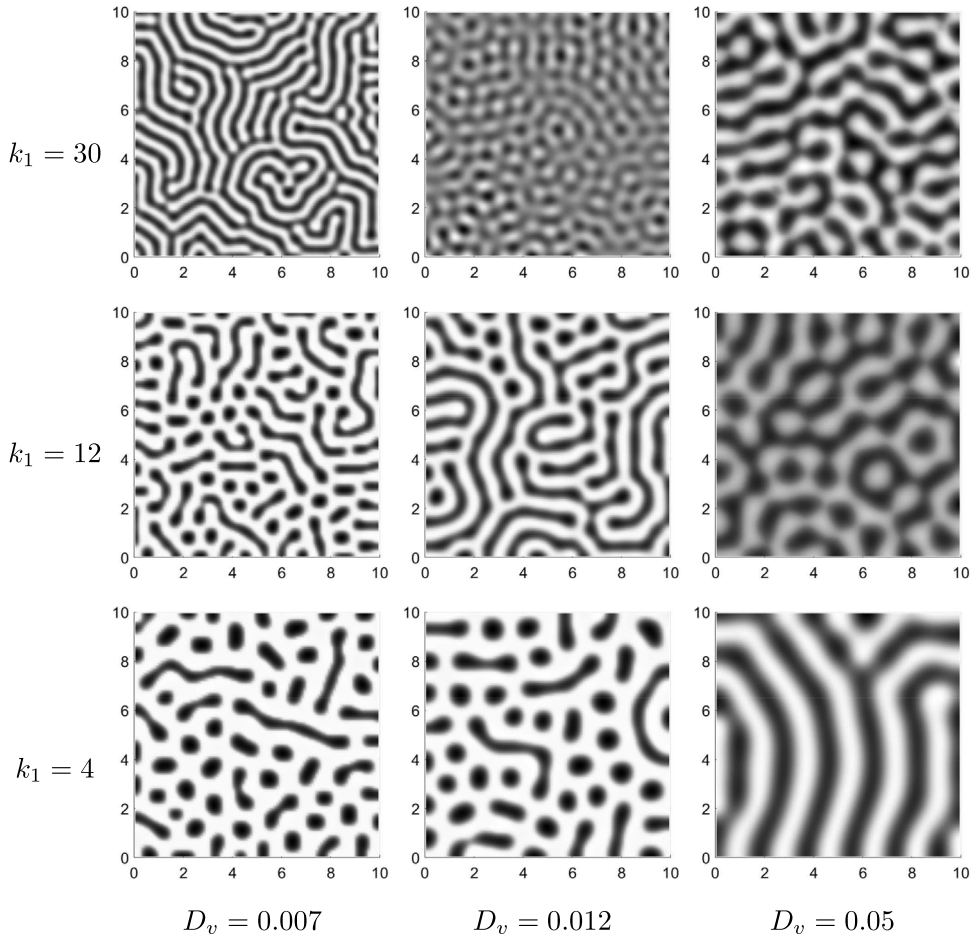

Fig. 2. Different pattern formations with different k_1 and D_v values in the discrete governing equations at time $t = 100000\Delta t$. From top to bottom, $k_1 = 30,\ 12$, and 4 are used. From left to right, $D_v = 0.007,\ 0.012$, and 0.05 are used. Here, $D_u = 1$ and $k_2 = 11$ are fixed.

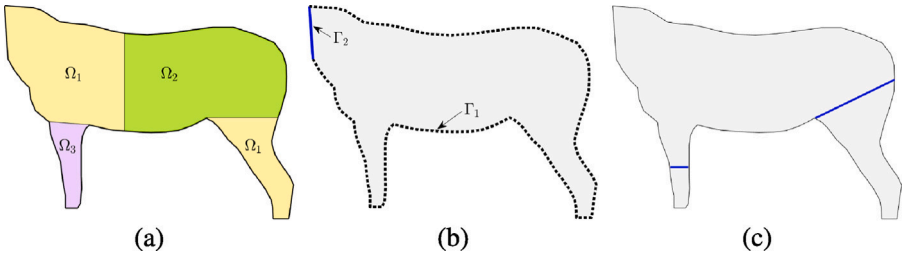

Fig. 3. Schematic illustrations: (a) Ω_1, Ω_2, and Ω_3 are subdomains where different parameter values are defined, (b) Γ_1 and Γ_2 are Dirichlet domain boundaries, and (c) two line segments where initial trigger values are defined.

investigating different pattern formation process of the three main species of zebra such as E. burchelli, E. zebra, and E. grevyi [13]. Because a cross-diffusion term in the system of the governing equations can play an important role in the formation of patterns [25], in the future study we will investigate its effect on the pattern formation.

CRediT authorship contribution statement

Junxiang Yang: Methodology, Software, Validation, Formal analysis, Investigation, Writing – original draft, Writing – review & editing, Visualization, Funding acquisition. **Junseok Kim:** Conceptualization, Methodology, Validation, Formal analysis, Investigation, Writing – original draft, Writing – review & editing, Supervision, Project administration, Funding acquisition.

Declaration of competing interest

The authors declare that they have no known competing financial interests or personal relationships that could have appeared to influence the work reported in this paper.

Data availability

Data will be made available on request.

Acknowledgments

The corresponding author (J.S. Kim) was supported by the Brain Korea 21 FOUR through the National Research Foundation of Korea, South Korea funded by the Ministry of Education of Korea. The authors

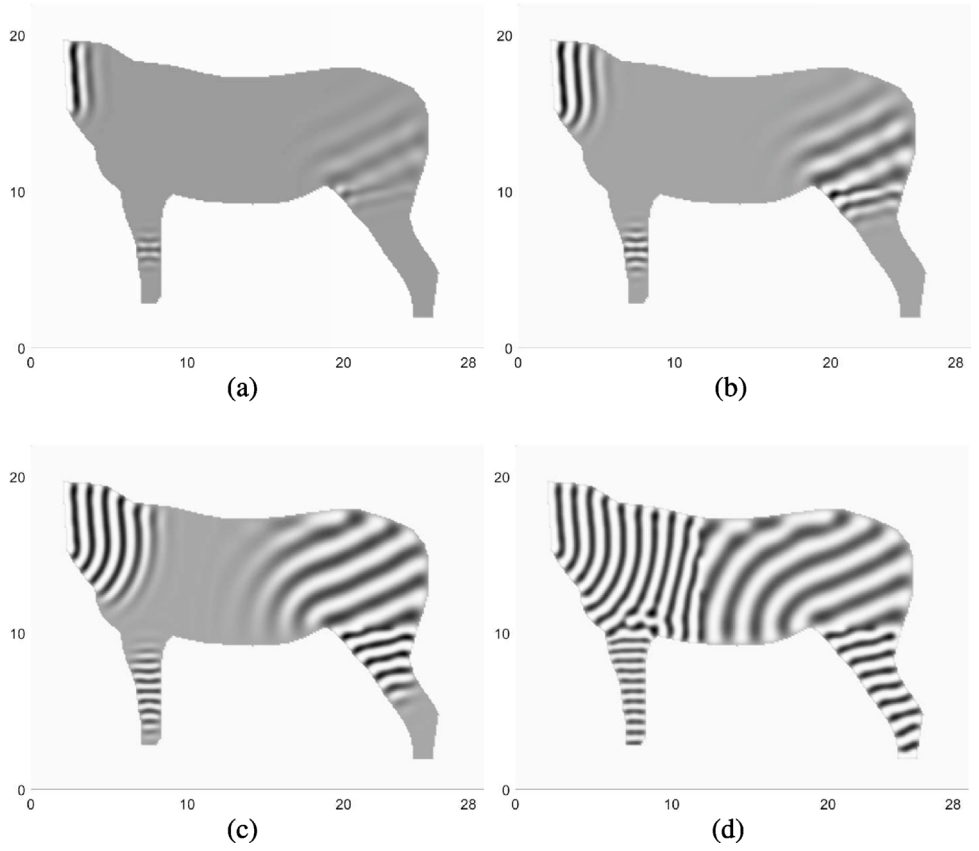

Fig. 4. (a)–(d) are snapshots of the temporal evolution of the zebra pattern formation at times $t = 10000\Delta t$, $15000\Delta t$, $25000\Delta t$, and $70000\Delta t$, respectively.

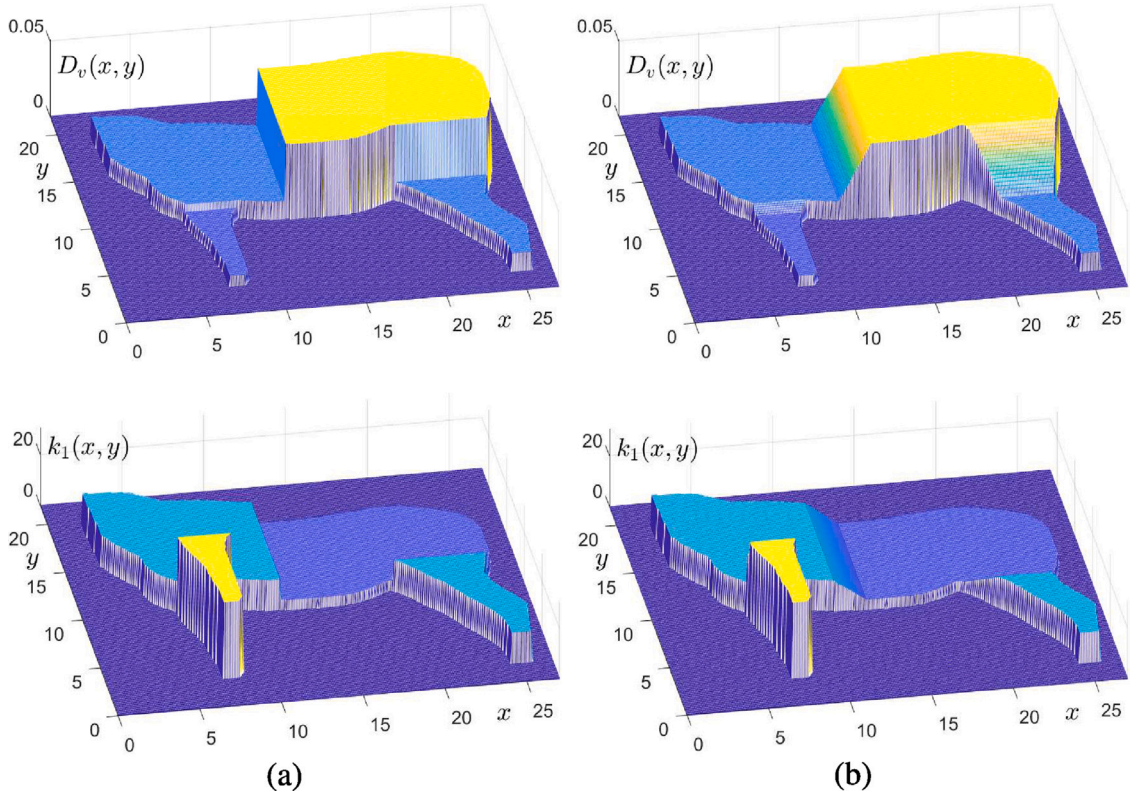

Fig. 5. Comparison of two methods of the space-dependent parameters: (a) sharp jump and (b) smooth profiles. Here, the top and bottom rows are $D_v(x,y)$ and $k_1(x,y)$, respectively.

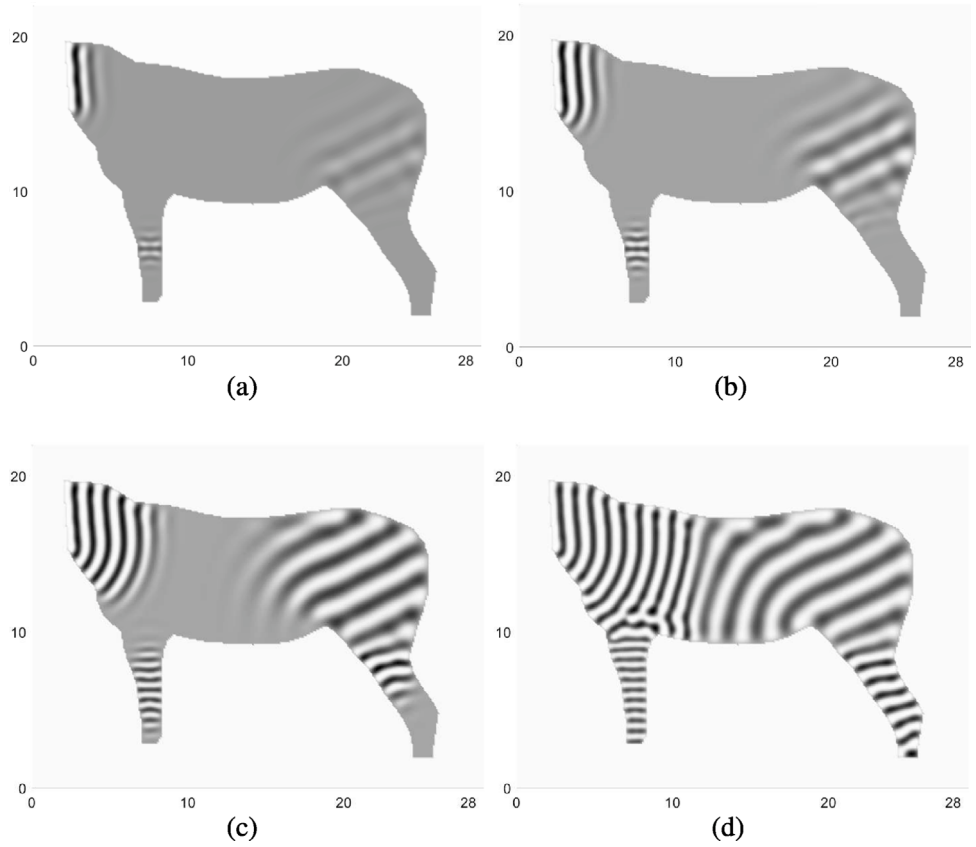

Fig. 6. (a)–(d) are snapshots of the temporal evolution of the zebra pattern formation at times $t = 10000\Delta t$, $15000\Delta t$, $25000\Delta t$, and $70000\Delta t$, respectively. Here, we used the smooth space-dependent parameters $D_v(x, y)$ and $k_1(x, y)$ as shown in Fig. 5(b).

would like to thank the reviewers for their valuable suggestions and comments to improve the paper.

References

[1] Maini PK, Woolley TE. The turing model for biological pattern formation. New York: Springer; 2019, p. 189–204.
[2] Manna K, Banerjee M. Spatiotemporal pattern formation in a prey-predator model with generalist predator. Math Model Nat Phenom 2022;17:6.
[3] Dey S, Banerjee M, Ghorai S. Analytical detection of stationary turing pattern in a predator–prey system with generalist predator. Math Model Nat Phenom 2022;17:33.
[4] Gulati P, Chauhan S, Mubayi A, Singh T, Rana P. Dynamical analysis, optimum control and pattern formation in the biological pest (EFSB) control model. Chaos Solitons Fract 2021;147:110920.
[5] Mittal RC, Kumar S, Jiwari R. A cubic B-spline quasi-interpolation algorithm to capture the pattern formation of coupled reaction–diffusion models. Eng Comput 2022;38:1375–91.
[6] Dats E, Minaev S, Gubernov V, Okajima J. The normal velocity of the population front in the Predator–Prey model. Math Model Nat Phenom 2022;17:36.
[7] Patterson LB, Parichy DM. Zebrafish pigment pattern formation: insights into the development and evolution of adult form. Annu Rev Genet 2019;53:15–56.
[8] Tarnita CE, Bonachela JA, Sheffer E, Guyton JA, Coverdale TC, Long RA, Pringle RM. A theoretical foundation for multi-scale regular vegetation patterns. Nature 2017;541:398–401.
[9] Konow C, Somberg NH, Chavez J, Epstein IR, Dolnik M. Turing patterns on radially growing domains: experiments and simulations. Phys Chem Chem Phys 2019;21:6718–24.
[10] Andrade-Silva I, Bortolozzo U, Clerc MG, González-Cortés G, Residori S, Wilson M. Spontaneous light-induced Turing patterns in a dye-doped twisted nematic layer. Sci Rep 2018;8:1–8.
[11] Halatek J, Frey E. Self-organization principles of intracellular pattern formation. Phil Trans R Soc B 2018;373:20170107.
[12] Owolabi KM. Computational analysis of different Pseudoplatystoma species patterns the Caputo–Fabrizio derivative. Chaos Solitons Fract 2021;144:110675.
[13] Jonathan BLB. A unity underlying the different zebra striping patterns. J Zool 1977;183:527–39.
[14] Perales-Graván CP, Lahoz-Beltra R. Evolving morphogenetic fields in the zebra skin pattern based on Turing's morphogen hypothesis. Int J Appl Math Comput Sci 2004;14:351–61.
[15] Jeong D, Li Y, Choi Y, Yoo M, Kang D, Park J, Choi J, Kim JS. Numerical simulation of the zebra pattern formation on a three-dimensional model. Phys A 2017;475:106–16.
[16] Rasheed SM. Pattern formation for a new model of reaction-diffusion system. In: 2018 International conference on advanced science and engineering. 2018, p. 99–104.
[17] Gravân C, Lahoz-Beltra R. Evolving morphogenetic fields in the zebra skin pattern based on turing's morphogen hypothesis. Int J Appl Math Comput Sci 2004;14:351–61.
[18] Kim H, Yun A, Yoon S, Lee C, Kim JS. Pattern formation in reaction–diffusion systems on evolving surfaces. Comput Math Appl 2020;80:2019–28.
[19] Lengyel I, Epstein IR. Modeling of Turing structure in the Chlorite–Iodide–Malonic acid–Starch reaction system. Science 1991;251:650–2.
[20] Kondo S. The reaction–diffusion system: a mechanism for autonomous pattern formation in the animal skin. Genes Cells 2002;7:535–41.
[21] Bard JBL. A model for generating aspects of zebra and other mammalian coat patterns. J Theor Biol 1981;93:363–85.
[22] Gormantara A, Pranowo. Parallel simulation of pattern formation in a reaction–diffusion system of FitzHugh–Nagumo using GPU CUDA. In: AIP conference proceedings. Vol. 2217. AIP Publishing LLC; 2020.
[23] Othmer HG, Painter K, Umulis D, Xue C. The intersection of theory and application in Elucidating pattern formation in developmental biology. Math Model Nat Phenom 2009;4:3–82.
[24] Murray JD. Mathematical biology II: spatial models and biomedical applications. Vol. 3. New York: Springer; 2001.
[25] Liu H, Ge B. Turing instability of periodic solutions for the Gierer–Meinhardt model with cross-diffusion. Chaos Solitons Fract 2022;155:111752.